

The Structural Changes of Hydrothermally Treated Biochar Caused By Ball-Milling

A Major Qualifying Project

Submitted to the faculty

Of the

Worcester Polytechnic Institute

For partial fulfillment of the requirements for the

Degree of Bachelor of Science

By

Erin Heckley

Joseph Toto

Juan Mauricio Venegas

May 1, 2014

Approved:

Professor Michael T. Timko, Advisor

Abstract

Glucose was hydrothermally treated to produce an amorphous oxygenated carbon structure known as biochar. Ball-milling was used to generate structural changes on the biochar and the time-dependence of these changes was studied. Raman spectroscopy was the primary tool for these studies, with additional Electron-spin resonance experiments carried out to verify structural changes. Ball-milling appears to produce enough strain on the char to generate defect sites. These radical sites accumulate with extended ball-milling time and form new locally stable structures within the char. Utilizing the radical molecules prior to their stabilization may be a new approach to greener functionalization of carbon-based catalysts.

Table of Contents

Abstract	2
Introduction	4
Experimental:	10
Biochar Preparation via Hydrothermal Carbonization:	10
Ball Milling Process:	10
Raman Spectroscopy	11
Electron Spin Resonance Spectroscopy	16
Initial Steps: Char Synthesis and Characterization	17
Error and Uncertainty Considerations	19
Results and Discussion	22
Time Study	22
Electron Spin Resonance Spectroscopy (ESR)	27
Defect Stability Study	28
Recommendations	31
Char Synthesis	31
Time Study	31
ESR	33
Defect Stability Study	34
Future Directions	34
Conclusion	35
Acknowledgements	35
Works Cited	36

Introduction

Anthropogenic contribution to global climate change is now widely accepted amongst the scientific community.¹ As one of the primary greenhouse gases, carbon dioxide is a major contributor to human-induced climate change. Increasing amounts of carbon trapped in the earth's ozone layer contribute to a greenhouse effect, which is predicted to increase the average U.S. temperature by 4 to 11 degrees Fahrenheit by 2100.² Human emissions of carbon dioxide are primarily due to fossil fuel combustion in transportation and power generation, which combined to total 5.3 billion metric tons of CO₂ emissions in 2012.³ Yearly emissions in the United States have been slowly decreasing due to reduced coal production and increased natural gas use, but worldwide, carbon emissions are still increasing. This makes reduction of carbon dioxide emissions an urgent need. To decrease carbon dioxide emissions, different approaches have been studied such as capturing the carbon dioxide produced in power plants, using carbon free energy sources such as solar and wind power, and switching to reduced-carbon fuels such as natural gas or biomass-derived fuels.

Since fossil fuel resources are finite, carbon sources based on lignocellulosic biomass may be a low-carbon and sustainable alternative to petroleum for both fuels and chemical applications. Biomass-based energy and materials have the potential to decrease greenhouse gas effects and can be generated locally to reduce energy required for transportation.⁴ The worldwide prevalence of agriculture ensures the sustainability of carbon feedstocks derived from biomass. Moreover, potential economic issues, which have arisen in the past due to short-term shortages in fossil fuels, could be avoided by the increased use of lignocellulosic biomass. Additionally, the conversion processes of biomass sources yield much less toxic waste during production than fossil fuels such as oil or coal as well as releasing far fewer pollutants to the atmosphere.⁴

Besides being useful as fuels, biomass has important structural properties that make it attractive as a chemical feedstock. The high oxygen content of biomass suggests that it can be made into a variety of materials such as plastics and specialty chemicals that can be modified to obtain various properties. This versatility has the potential to allow fossil fuel feedstocks to be supplemented by biomass in the chemical industry. However, the use of biomass as a chemical resource presents some problems, mainly due to the difficulty of breaking cellulose and hemicellulose into usable sugars. Current methods rely on high temperature pyrolysis⁵ or acid-based de-polymerization.⁶ These often require harsh conditions that can generate toxic by-products or require energy intensive operations. Milder conditions can be used in the presence of a catalyst, but these often require metals of limited supply⁷ or expensive ionic liquid solvents.⁸ Dilute solutions of biomass feedstock are common in these methods, making biofuel production an extremely water intensive process that requires expensive downstream separation steps for product recovery.⁶

Finding biomass conversion technologies that are feasible to scale up for wide spread applications and are environmentally friendly is necessary to ensure the sustainability of biomass as an effective replacement for non-renewable carbon sources. Green chemistry is a current area of study that can provide guidelines for this task. Anastas and Warner define green chemistry as, "The utilization of a set of principles that reduces or eliminates the use or generation of hazardous substances in the design, manufacture, and application of chemical products."⁹ Green chemistry also advocates the minimization of waste, solvent use, and energy consumption, all of which could lead to economical benefits in biomass treatment processes. Table 1 lists some of the guidelines that should be followed to ensure green chemistry practices.

Table 1: Guidelines for Green Chemistry

Principles of Green Chemistry

1) Prevention

- It is preferable to prevent waste than to treat it

2) Atom Economy

- Synthesis should maximize the use of all materials incorporated into the process

3) Production of Safer Chemicals

- Chemical products should carry out their function while minimizing their toxicity

4) Minimal Solvent Use

- Use of solvents should be eliminated when possible or minimized

5) Energy Efficiency

- Energy requirements should be considered for their economical and environmental impacts, and thus minimized

6) Renewable Feedstocks

- Raw materials should be obtained from renewable sources when possible

7) Catalysis

- Catalytic reagents are preferred over stoichiometric reagents

• *(Adapted from Anastas & Warner, 1998)*

Based on these guidelines, catalysts for green biomass processing must be: 1) stable to ensure long-term reusability, 2) retain high activity at relatively mild conditions to avoid high-energy consumption, 3) sourced from renewable resources and manufactured using low-energy methods. With this mindset, catalysts synthesized from biomass sourced feedstocks might provide a cost effective option, at least for certain applications. Carbon's widespread availability from biomass could ensure a cheap supply of catalysts for large-scale operations. Depending on the synthesis conditions, carbon materials can exhibit many features required of active catalysts, including high surface areas and high density of acid sites.¹⁰ Carbon is also versatile; it can be functionalized in various ways to suit the particular needs of a process. Several functional groups can be introduced to the surface, and the catalyst surface can be modified by either liquid or gas phase processes.^{11 12} A common functionalization procedure is the use of fuming H₂SO₄ to insert sulfonic acid groups onto the carbon surface. Sulfonation creates acidic surface groups that act as active sites for promoting reactions including the hydrolysis and dehydration steps that are important steps in biomass processing. In addition to making the carbon surface more

active, acid treatment changes the surface polarity, rendering it hydrophilic, which is beneficial when using water as a solvent.¹² Unlike traditional mineral acid catalysts such as HCl or H₂SO₄, carbon is a solid-acid catalyst, which makes its recovery relatively simple and can simplify downstream product processing operations by omitting acid extraction processes.⁶

While carbon has many benefits, its reactivity is often not as high as zeolites or sulfonated metal oxide systems. Although it imparts catalytic activity, functionalization is often done under harsh conditions that are inconsistent with green chemistry principles. An alternative approach to enhancing carbon activity is mechanochemical processing, which is the activation of chemical reactions by the application of mechanical energy. Mechanochemical processing changes the surface and the subsurface properties of the material such as surface area and the number of active catalytic sites. Within the mechanochemistry field, ball-milling is of particular interest in catalyst preparation since it can be performed using simple laboratory equipment. During ball-milling, a container filled with the catalyst material and milling balls is shaken at high frequencies of 60Hz and higher. The energy added by these vibrations is transferred to the bearings, which in turn impact the catalyst material.

Ball-milling has proved to be effective for preparing materials with enhanced reactivity.¹³ Theoretical analysis suggests that ball-milling impacts can generate temperatures around 1000°C¹⁴ and pressures above 1GPa.¹⁵ These localized conditions can provide enough energy to break carbon-carbon bonds by inducing a high strain rate, thus creating defect sites in the catalyst.¹³ Ball-milling for extended amounts of time can completely disrupt the carbon structure.¹⁶ The defect sites are highly reactive, and can be used to catalyze other reactions, or they can be used to transform the carbon catalyst with various functional groups. The ball milling method has been used to introduce hydroxyl functional groups to the carbon surface by milling carbon with KOH¹⁷ and nitrogen functional groups by milling under an N₂ atmosphere.¹⁸ This kind of flexibility is desirable as an alternative to wet reaction conditions and follows desired green chemistry practices.

Despite the successful use of ball-milling in catalyst synthesis, the process mechanism is only beginning to be understood. In a recent study by Immohr et al., CO oxidation reactivity slowly increased to a maximum after 500 minutes but upon stopping the ball mill, rapidly dropped.¹⁹ This may indicate that ball-milling causes only temporary defects in the catalyst that are quickly reformed. The observed ball-milling reactivity was an order of magnitude greater than that observed for the unmilled catalyst, suggesting the potential of ball-milling as a catalyst preparation tool. Furthermore, the catalyst activity did not return to its original reactivity once milling was stopped, indicating other lingering effects caused by ball-milling. Studies by Milev, et al. indicate that milling does produce lasting effects upon carbon, including a change in carbon geometry from sp_2 to sp_3 and sp .¹⁵ Milev argues that the carbon-carbon bonds that are broken by ball-milling are quickly reformed after ball-milling stops.¹⁵ Understanding these lasting effects could aid in preparing active catalysts under mild processing conditions.

Finding a way to maintain the catalyst reactivity observed by Immohr et al.¹⁹ could provide important insight on the transformations that take place during and after ball-milling, while simultaneously creating alternative pathways for catalyst preparation. Xing, et al. noted that the temporary defect sites created during ball-milling are highly reactive. Specifically, they observed that recently milled graphite reacts explosively with oxygen on contact with air.²⁰ Controlled functionalization of these active sites could maintain their activity while stabilizing the catalyst for use in other chemical processes.

The present study is a scientific investigation of the structural changes that a char material undergoes during ball-milling treatment. The primary goal is to determine the effects the ball milling procedure has on amorphous carbonaceous material over the course of time. Key outstanding questions in this field are: 1) the influence of ball milling time (or energy) on carbon structural characteristics and the rates at which defects can be generated during ball milling and 2) the time required for ball-milling-induced defects to repair. Specifically, the study was designed to determine whether defects caused by ball-milling only last short periods of time or whether ball-milling causes stable changes in carbonaceous material. To achieve this objective, ball-milling experiments were done on

glucose-derived biochar to determine the effects that ball-milling time has on carbon structures. Glucose was chosen as a representative renewable carbon resource, though similar work has been performed with cellulose, biomass, and many wastes.^{21 22 23} The primary characterization method was Raman microscopy as this tool has been utilized in previous studies to elucidate the structures of carbon materials.^{24 25 26} In addition to structural characterization immediately following ball-milling, carbon materials were studied at specific times following the ball-milling treatment to determine the time scales of repair for the structural defects introduced during ball milling. This work provides a stronger rationale basis for future development of carbon catalyst modification methods that can provide inexpensive and environmentally friendly access to biomass-derived chemicals and fuels.

Experimental:

Biochar Preparation via Hydrothermal Carbonization:

Hydrothermal carbonization is a technique that uses water as a reaction medium for the conversion of saccharides to solid carbonaceous material.²⁷ This process allows for the formation of carbon-rich solid char containing a high concentration of reactive oxygen functional groups.²⁸ Preparing the carbon char samples to be tested and characterized began with mixing a solution consisting of 39.6 g of glucose powder in 160 mL of distilled water based on the procedure described by Guo.¹¹ The flask was constantly mixed while the glucose was added to prevent any residue from forming at the bottom of the container. After mixing, 100 mL of the solution was poured into a 160 mL Teflon-lined stainless steel autoclave, pressure sealed, and placed in an oven at 180°C for 5 hours. Once the 5 hours were completed and the vessel cooled, the char was collected, washed, and filtered using ethanol and water three times with 40mL of each. Once the filtration liquid remained was clear, the char was dried overnight in a petri dish in an oven set to 80°C. The dried char was then ground into a fine powder using a mortar and pestle and stored in vials until samples were ready to be tested or used in other experiments.

Ball Milling Process:

Sample Preparation:

0.5 grams of char was placed in a stainless steel ball-milling vessel in an atmospheric environment. Following the loading procedures recommended by the ball mill vendor, 1/3 of the vessel was filled with the sample being ball milled, 1/3 filled with the grinding balls, and the last 1/3 left empty.²⁹ Based on results reported by Immohr et al.,¹⁹ two 5 mm diameter stainless steel balls separated by one 10 mm diameter ball were put in the vessel, as shown schematically in Figure 1. Immohr et al, observed that this configuration resulted in the most significant increase in the reaction rate of several tested.¹⁹ The vessel was sealed to prevent sample leakage using a rubber O-ring between the lid and the bottom of the jar and insulating tape. The vessel was loaded into a Retsch MM200 mixer mill and the sample was milled for the desired amount of time at a frequency of 60 Hertz.

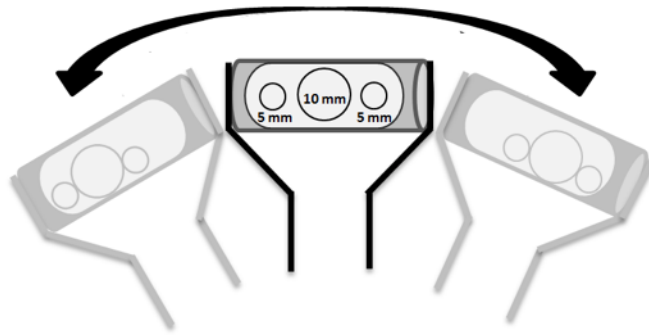


Figure 1: Schematic of the Ball Milling Method Used

Studies:

Two ball mill time studies were completed: one varied the duration of ball milling time and the other focused on the changes of ball-milled material with respect to time after milling. The first study was done by ball milling char for 30, 60, 90, 120, 180, and 300 minutes and analyzing the material using Raman spectroscopy using a Horiba XploRa Raman spectrometer. Each time point was repeated three times to obtain representative statistics. Additionally, each sample was scanned in three locations to ensure that the scans were representative. The Raman study was conducted as soon as the material was taken out of the ball mill, approximately 5 minutes afterwards. This time study was completed to investigate the structure of the char as a function of ball milling time.³⁰ The second study that was carried to determine whether the defects caused by ball-milling remained stable with time or if they degraded into new structures. The second study was performed by ball milling char for 90 minutes and then running consecutive Raman studies every fifteen minutes for 2 hours and then every hour after that for 4 hours. This study was completed to further analyze char's reactivity and particle size after time has passed to gain insight on the short and long term effects of milling.

Raman Spectroscopy

Raman scattering is a vibrational phenomenon caused by alterations in the electric field of a molecule when it is excited by monochromatic light. This interaction causes a perpendicular scattering of the light source that can be elastic or inelastic in nature. If the detected light has the same frequency as the incident beam, the scattering process is considered elastic. This type of vibrational phenomena is known as Rayleigh scattering. If the detected light has a different frequency than the incident beam, it is considered Raman scattering.³¹

The change in frequency of the detected light is known as the Raman shift, and its intensity and location can provide insight into the molecular structure of a compound. Raman and infrared (IR) spectroscopy differ in the wavelengths and phenomena that are used, but they are complementary techniques to ensure the maximum amount of information on a compound is obtained. IR excels at characterizing polar bonds, while Raman is an important tool in understanding symmetrical structures within a compound. As an example, C=C, S-S and C-S bonds produce weak peaks in IR and strong peaks in Raman.³¹

Raman spectroscopy then, serves as a fundamental tool in the analysis of synthesized biochars. Due to the symmetry of carbon-carbon bonds, Raman provides insight on the nature of the carbon structure of the studied molecules. As a focus of traditional Raman studies, two primary peaks have been identified, typically labeled “D” and “G”. These peaks have been studied extensively in graphitic compounds due to the high degree of order in the carbon structure of this material. Figure 2 provides representative Raman spectrum of graphite for reference.

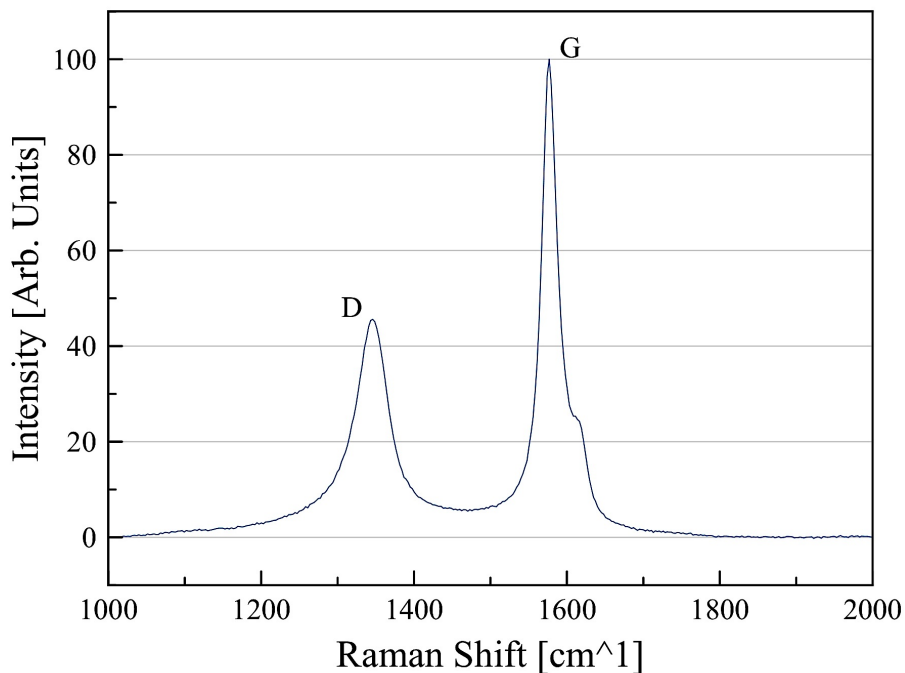


Figure 2 - Graphite Raman Spectrum (Normalized to 100% G peak intensity)

Reich and Thomsen³² consider the D peak at a wavenumber around 1,350 cm⁻¹ to indicate the presence of defects in the carbon structure. Milev, et al. further developed this description by describing the D peak intensity to be proportional to the presence of hexagonal ring

structures within the graphite.¹⁵ Moreover, the broadness of this peak reflects the overall cluster size containing hexagonal ring structures.¹⁵ The G peak at 1575 cm⁻¹ on the other hand, describes the unconjugated *sp*² carbon bonds within the graphite.¹⁵ The shoulder on the G peak at around 1650 cm⁻¹ is known as the D' peak and is seen only in the presence of disorder in the graphite. This peak however, may be hard to deconvolute after extended milling.³³

Historically, Raman analysis of carbon-rich compounds has focused on the D/G ratio as a measure of disorder in a sample.^{26 15 30 24} This analysis however, is commonly done on graphitic carbon samples, which have a noticeably different structure from biochars. The graphite presents sharp, well-defined peaks while the biochar has broad peaks with far lower intensities. A comparison of biochar and graphite peaks can be seen in Figure 3. Although having some qualitative similarities, the D and G peaks obtained from biochar have enough qualitative differences that the features are unlikely to have the same physical meaning for both carbon types. Li, et al³³ developed new physical interpretations for the Raman spectra of amorphous carbon structures³³ using amorphous carbons similar to the biochars which were synthesized as previously described. Specifically Li, et al³³ fit the amorphous carbon Raman spectrum to 9 distinct molecular structures, as shown in Table 3.

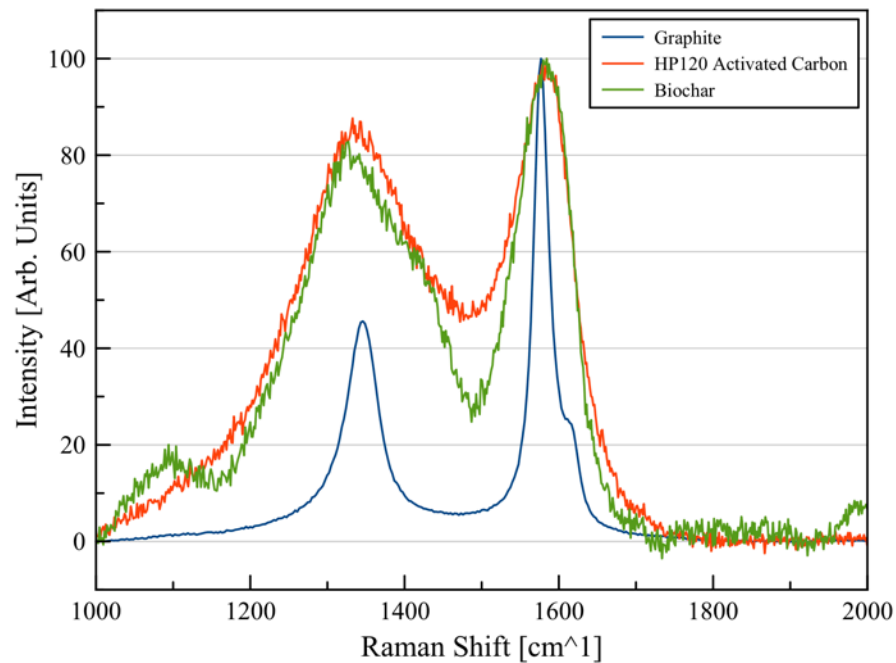


Figure 3: Raman spectra of graphite, biochar, and an activated carbon ((Normalized to 100% G peak intensity)

)

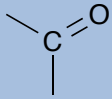
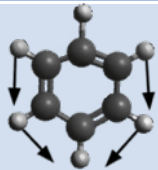
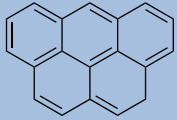
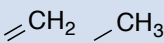
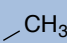
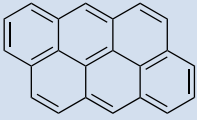
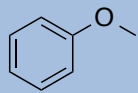
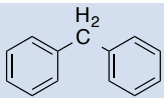
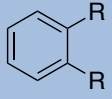
For all studies, a Horiba XploRa Raman spectrometer was used. Table 2 summarizes the settings used for all experiments. Don't break paragraphs to insert figures or text, unless the break occurs over a page break.

All spectra were baseline corrected and normalized to the G peak intensity using LabSpec6 software provided by Horiba. Magic Plot, a commercial software, was used to fit the peaks contained in the spectra, as seen in Figure 3. The full width at half maximum, areas and intensity values for the G, G_r, V_r, V_i, D, S, S_r, and G_i peaks were determined by automatically setting each peak's band position based on Table 3 provided by Li et al.⁸ The peak intensities were then manually adjusted to best fit each individual spectrum and all peaks were assumed to be Gaussian. Figure 4 shows a representative Raman spectrum of biochar, showing both the raw data and the best-fit curves

Table 2: Raman Spectrometer Settings

Setting	Used Value
Laser Wavelength	532nm (10% power)
Accumulation time	5 seconds (50 accumulations per scan)
Scan range	800-220cm ⁻¹
Grating	1800
Slits	300
Holes	100

Table 3: Peak Assignment (adapted from Li, et. al) *(R) denotes residual peak fits.

Band Name	Position [cm ⁻¹]	Description	Structure
G _L (R)	1700	Carbonyl group	
G	1590	Aromatic ring quadrant breathing, alkene C=C	
G _R	1540	Aromatic chains with <6 rings	
V _L	1465	Methylene & methyl groups, amorphous carbon structures	
V _R	1380	Methyl group, amorphous carbon structures	
D	1300	Aromatic chains with 6 or more rings	
S _L (R)	1230	Aryl-alkyl ether	
S	1185	C-C bonds between alkyl and aryl structures	
S _R (R)	1060	Substituted benzene ring	

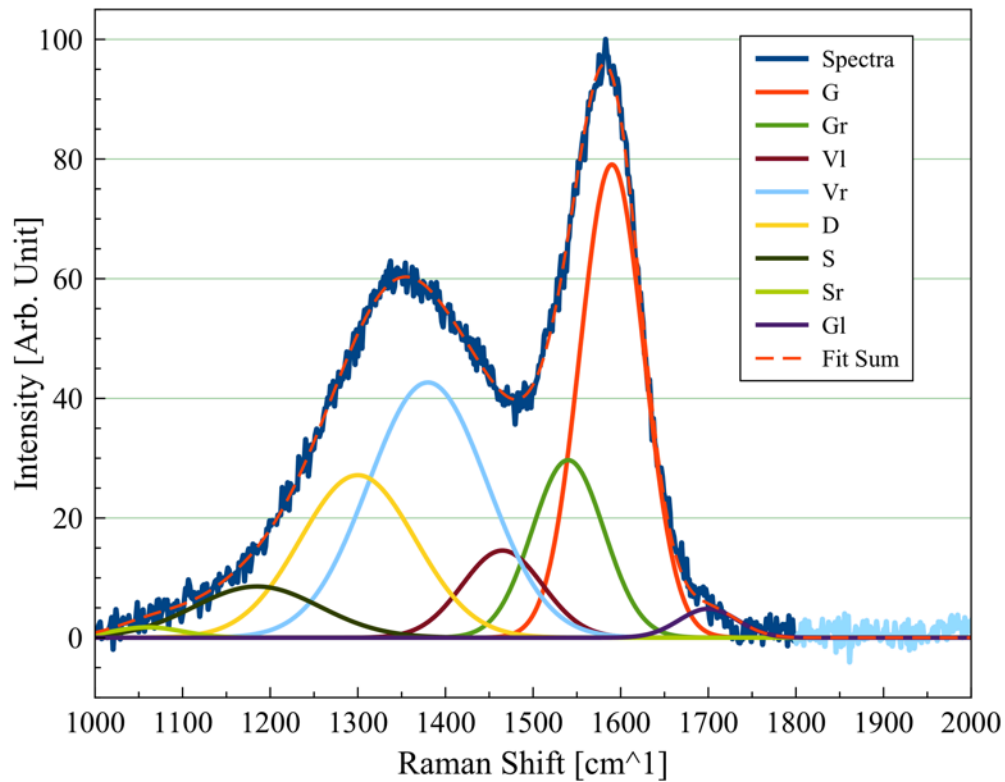


Figure 4: Peak fitting of char ball-milled for 60 minutes (Normalized to 100% G peak intensity)

Electron Spin Resonance Spectroscopy

Raman vibrational measurements were complemented using electron spin resonance (ESR). ESR has been used to characterize paramagnetic surface groups and clarify their role in electrochemical reactions. This should have reference citations ESR measurements of carbon can provide information on structural and electronic properties that depend on crystalline size, impurities, preferred orientation, and preparation procedure.³⁴

ESR was used to measure free radical concentrations before and after ball-milling of the biochar. Paramagnetic structures such as free, unpaired electrons can be located in either the conduction bands or in the localized edge sites of the sample.³⁵ The ESR spectra were measured using a Bruker EMX ESR Spectrometer equipped with a 100 kHz field modulation and 1 G at 1 mW microwave power. Measurements were conducted using char samples ball-milled for 0 (as synthesized), 30, 120, and 300 minutes approximately five weeks after ball-milling. The 300-minute results were not used in future analysis due to presence of metal radicals in sample that showed radical contents orders of magnitude larger than expected.

This similar effect was previously observed in prior experiments conducted by Smith et al.³⁵ For all cases, the ESR magnets were held at an operating temperature below 20°C, The samples were placed within thin-walled, cylindrical quartz tubes that allow for desorption of energy from the radio-frequency field. A more recently ball-milled char sample (within 24 hours, ball-milled for 30 minutes) was measured to compare any potential differences between free radical degradation over the five weeks. Each of the spectrum obtained were normalized using sample mass for quantitative interpretation.

Initial Steps: Char Synthesis and Characterization

A review of the char formation mechanism will help to understand the changes caused by ball-milling,. A manifold of parallel and sequential reactions occur during hydrothermal biochar synthesis. Sevilla and Fuentes have developed a generalized reaction pathway for the conversion of glucose to biochar.²¹ This pathway has been adapted for this work and is presented in Figure 5.

As seen in the Figure 5, glucose forms different soluble products such as acetic, lactic and levulinic acids. These organic acids serve as catalysts for the subsequent breakdown of the glucose monomers through varied dehydration and fragmentation reactions. The products include aromatic compounds, furan compounds, and aldehydes. As the fragmentation reactions continue toward completion, polymerization and condensation reactions begin, thus leading to the formation of insoluble organic polymers. Finally, aromatization occurs and some additional dehydration reactions may occur to form carboxyl groups in the polymer chains.²¹

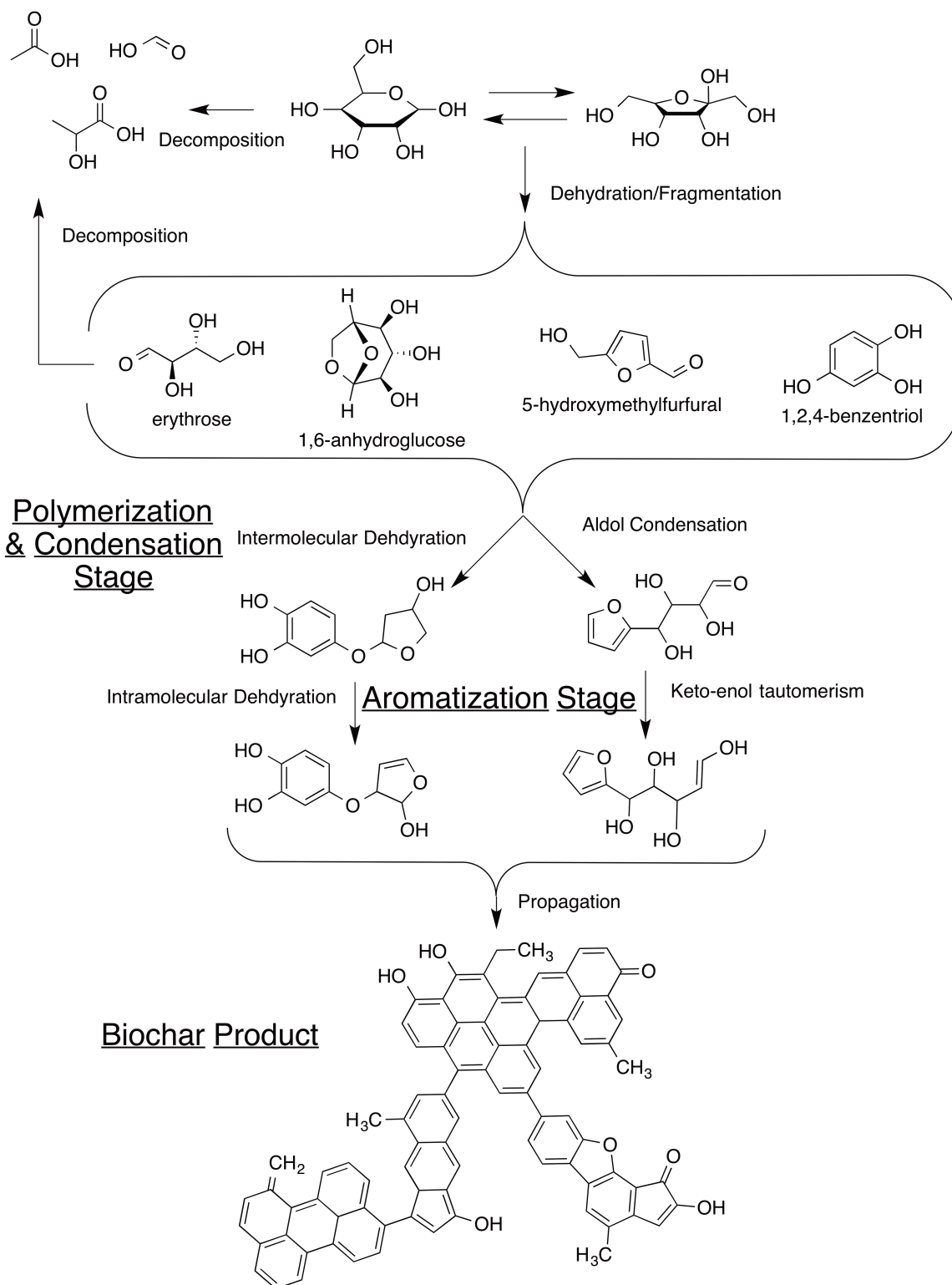


Figure 5: Glucose to biochar via hydrothermal synthesis (Adapted from Sevilla & Fuertes)²¹

Error and Uncertainty Considerations

Throughout the study, variations in the experimental data highlighted several key points of uncertainty. The synthesis of biochar from glucose and the proper aiming and use of the Raman spectrometer were the most critical sources of error. During hydrothermal synthesis, the biochar product varied from batch to batch in both quantity and characteristics. Figure 6 shows the Raman spectra of the 5 char batches that were used in all experiments. The Raman spectra show differences in both intensity and shape, indicating variations in the carbon groups present in the chars. These differences can be attributed to variations in the thermal treatment time and in the cleaning process. Despite ending the synthesis process after 5 hours of oven time, it was observed that some batches took longer to cool inside the oven. This could make the hydrothermal treatment proceed for different times with each batch. Additionally, some batches, in particular the batch with the lowest D band intensity in Figure 6, required repeated ethanol/water cleaning procedures to ensure the product was properly washed of other compounds. To account for these fluctuations in the biochar batches, repeat experiments were carried out for the time study to ensure that the observed trends were not a product of an individual batch, but a trend of the general biochar ball-milling process.

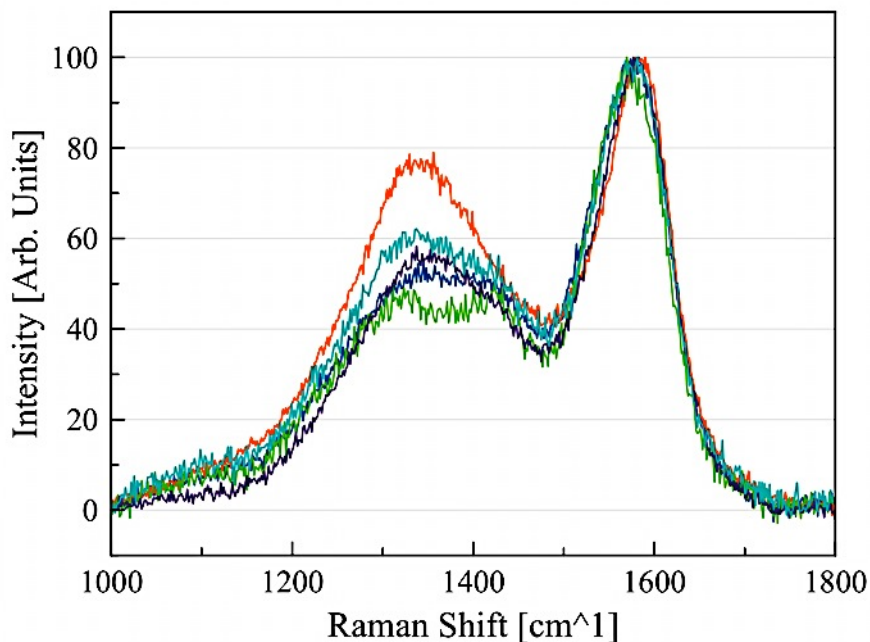


Figure 6: Raman Spectra of All of the Char Samples. Synthesized at 180°C for 5 hours (Normalized to 100% G peak intensity)

Raman scans at three different locations of the char sample were taken to understand the homogeneity of the sample. Care was taken to properly focus the Raman optics to ensure maximum spectral intensity. This manual aiming varied significantly with each sample and could have been a source of error in determining peak areas. Variations in intensity would be lost after the normalization of the spectrum with the G peak intensity. Additionally, the difference between the peak areas for each char sample was studied, and their deviations are shown in Table 4. Significant variations occur with the D and S peaks, which would prove critical in the study of the ball-milling process. To account for this variability, as well as for peak fitting variations in the experiments, propagation of error analysis was carried out on the peak ratios. The uncertainty of the ratio was determined using the equation³⁶

$$\sigma_{A/B}^2 = \frac{A}{B} \left[\left(\frac{\sigma_A}{A} \right)^2 + \left(\frac{\sigma_B}{B} \right)^2 - 2 \frac{\text{COV}_{AB}}{AB} \right]$$

Where A and B are the areas of the peaks of interest, $\sigma_{A/B}$ is the calculated uncertainty in the peak ratio, σ_A and σ_B are the standard deviations in the respective peak areas, and cov_{AB} is the covariance between the peaks. Using covariance, we can account for relationship between biochar structures and how the change in one affects others.³⁷

Table 4: Standard Deviation of Each Peak for Different Char

Peak Name	Average Area	Standard Deviation of Area	% of Average Area
G	6832.8	275.6	4
G _R	2972.5	202.2	6.8
V _L	2133.8	686.9	32
V _R	7006.6	1451.5	20
D	4577	820.7	17.9
S	1635.6	728.1	44.5

Raman spectra taken at different locations in the same char sample, as shown in Figure 7, indicate that, despite grinding and mixing, biochar has noticeable localized differences in its composition. This adds to the necessity of Raman studies of biochar to have large sample sizes that can show general trends irrespective of localized differences in a sample. The defect stability study required that Raman scans be taken on the same location in the biochar. Due to

this, no repeat experiments were available to carry out uncertainty calculations. Time constraints during the project did not allow additional defect stability studies to be carried out. Due to the discrepancies in un-milled char spectra, it is possible that the feedstock accounted for the largest source of variability in the experiments.

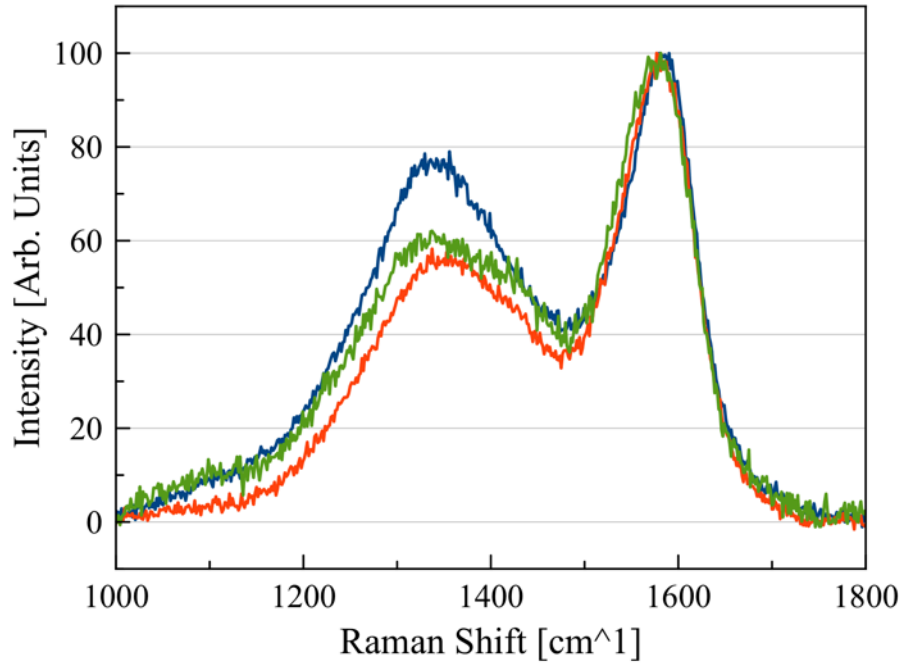


Figure 7: Variation in Raman spectra of three spots in same char sample (Normalized to 100% G peak intensity)

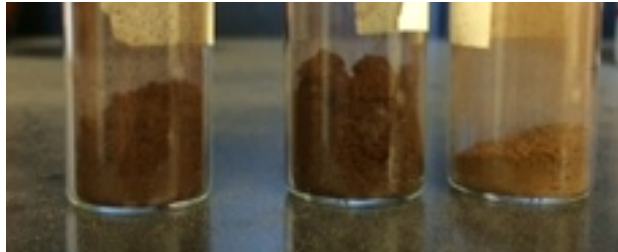


Figure 8: Comparison of Different Chars. All produced in the same oven at 180°C during 5 hours. The samples were not produced the same day.

Results and Discussion

By analyzing the peak ratios in the Raman spectra of ball-milled char for different periods, structural changes could be quantified and compared. The S/G and D/G_R ratios were of particular importance due to the physical structures they represent. The S/G provided information on the linking amongst the aromatic structures of biochar while the D/G_R described the aromatic structures themselves. To complement the findings in the Raman spectra, electron spin resonance studies gave information of free-radical presence in the biochar samples. For uniformity, all spectra were normalized to the intensity of the G band.

Time Study

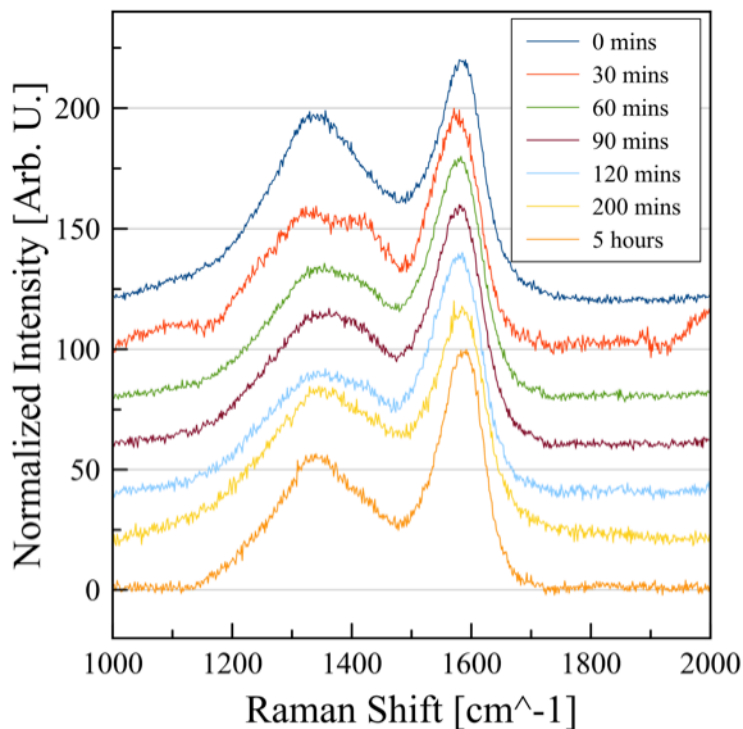


Figure 9: Raman spectra of ball-milled biochar (Normalized to 100% G peak intensity)

When comparing the un-milled sample and the sample milled for 30 minutes, an important difference can be observed in D band intensity between 1100 and 1700cm⁻¹, as seen in Figure 9. The un-milled sample has a sharper and more intense peak in comparison to the milled sample whose intensity is lower in the D peak. As described in the experimental section, Li, et al de-convoluted the Raman spectra of pyrolyzed brown coal.³³ This material is similar to biochar due to its carbon, hydrogen and oxygen contents so it may be possible to describe the

Raman spectra of biochar based on peak fittings developed for pyrolyzed coal. Table 3 shows the physical interpretations that could be given to the peak deconvolution.³³ Taking the ratios between several of these peaks, the changes occurring during different ball-milling times can be identified, and their physical meaning interpreted.

The general structure of biochar seen in Figure 5 shows large aromatic ring structures that are cross-linked by alkyl branches. Considering the high strain rate the biochar receives from ball-mill impacts¹³, the alkyl branches could be broken and generate radical bearing defect sites. The S band at 1165cm^{-1} has been determined to represent the C-C bond between aryl and alkyl carbons, and the S/G ratio can be taken as a measure of the relative presence of cross-linking alkyl branches in the aromatic ring structures. Figure 10 shows a decrease in the S/G ratio with ball-milling time, indicating a decrease in alkyl branches. Figure 13 shows this alkyl branch breaking as the initial step in a possible ball-milling reaction mechanism. It is possible to follow the ensuing reaction by analyzing different peak ratios in the Raman spectra.

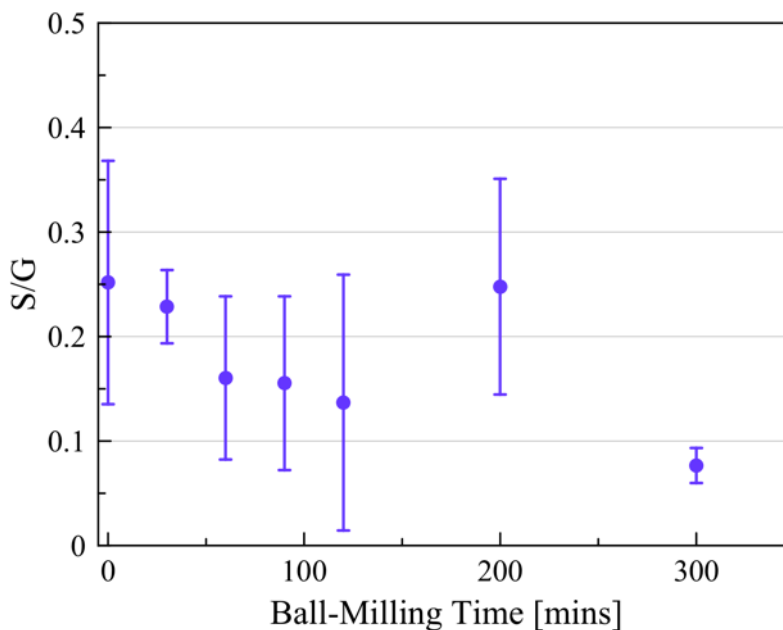


Figure 10: S/G ratio with ball-milling time

Studies have shown that structures with less than 6 aromatic rings in a chain produce no significant effect in the D band, but instead are seen in the G_R position at 1640cm^{-1} .³³ These are typically present in amorphous carbon along with methyl and methylene groups (V_L and V_R bands) that join different aromatic ring chains into clusters. Li³³ and other studies³⁸ have used

the ratio $D/(G_R+V_L+V_R)$ as a measure of the concentration of small, highly amorphous short chain clusters relative to those contained in more structured 6+ ring fused structures shown by the D band. Figure 11 shows how the $D/(G_R+V_L+V_R)$ ratio has noticeably increased after 5 hours of ball-milling, indicating an increase in the amount of longer, 6+ ring structures in the sample relative to the small, amorphous clusters.

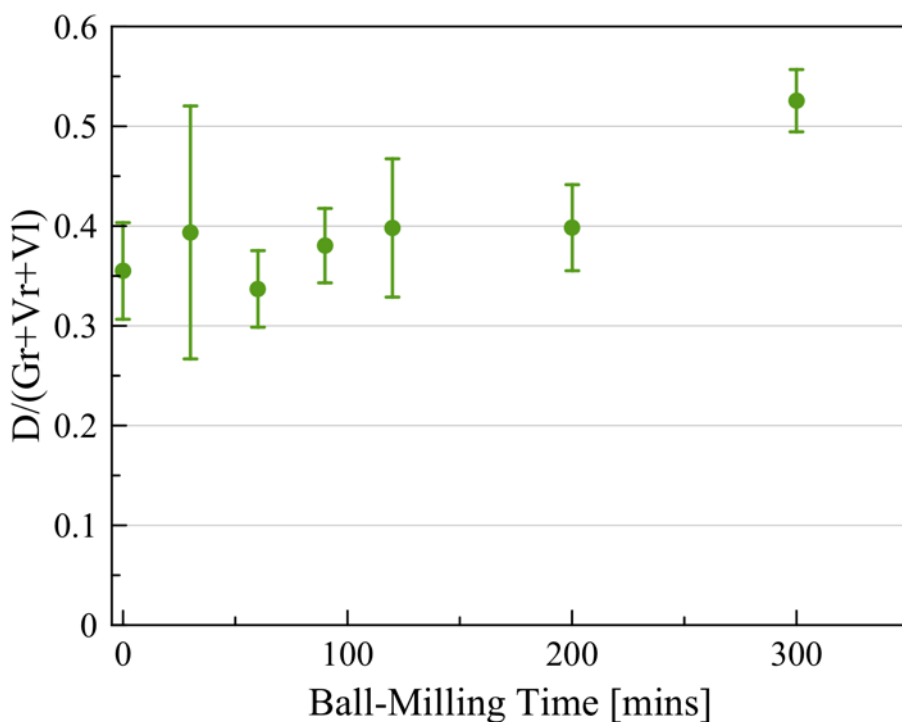


Figure 11: $D/(Gr+VI+Vr)$ ratio with ball-milling time

As ball-milling occurs, the force from the impacts can break the methyl and methylene groups connecting shorter aromatic structures generating reactive defect sites as observed in the S/G ratio analysis. These could then react amongst themselves and fuse into larger structures. Figure 13 shows this possible scenario in the leftmost structure after radical formation. Of particular interest in this process however, is the noticeable lag time between the start of ball-milling and a significant increase in the $D/(G_R+V_L+V_R)$ ratio. During the first 200 minutes of milling, the ratio is relatively stable. This could indicate that there is a period of radical molecule accumulation, and only after a large amount of radicals is present will the ball-milling cause reactions between defect sites to form stable 6+ ring chains. This “pool” of radical molecules could be a valuable resource in the functionalization of the biochar into more reactive carbon catalysts.

The transition between more amorphous short aromatic chains into longer, more locally organized ≤ 6 ring chains can be more clearly observed by comparing the D and G_R ratios. As seen in the $D/(G_R+V_L+V_R)$ ratio in Figure 11, it was expected that the D/G_R ratio would increase with milling time. Figure 12 shows that this is actually the observed result. From the three different peak ratio observations, Figure 13 can be understood as a process of radical formation followed by radical stabilization. This process is sped up with increasing radical content.

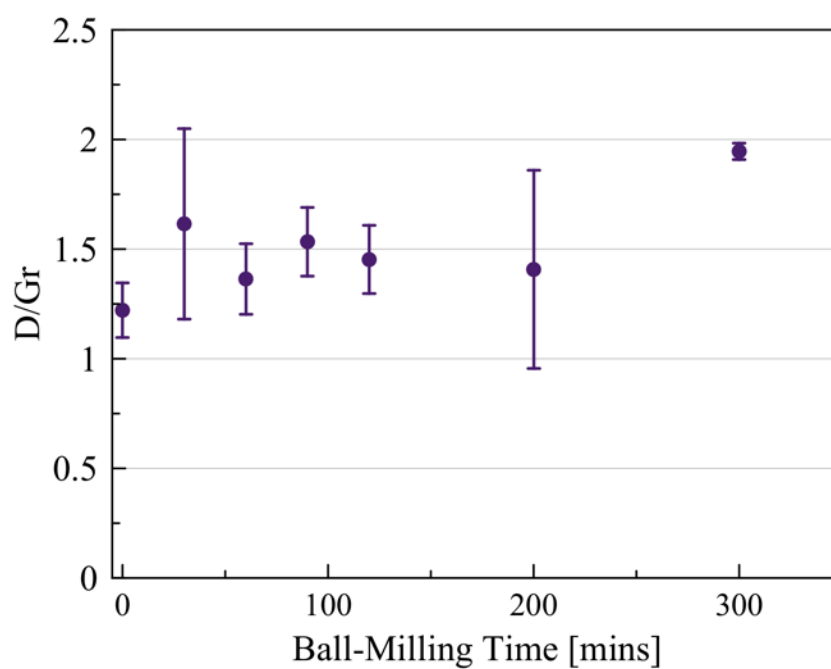
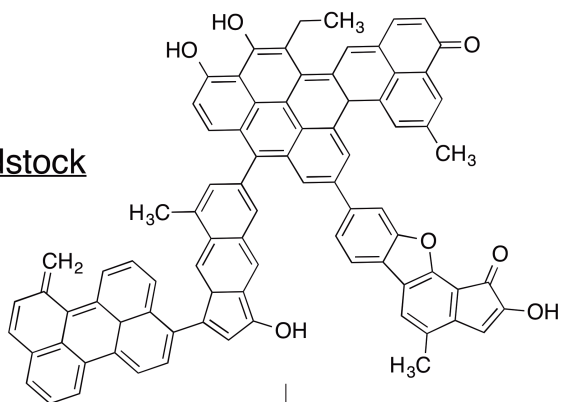


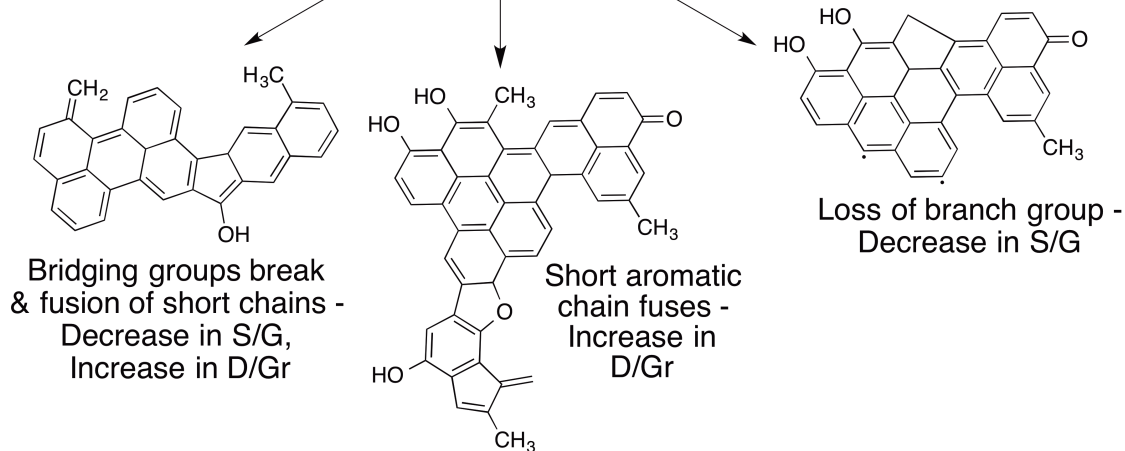
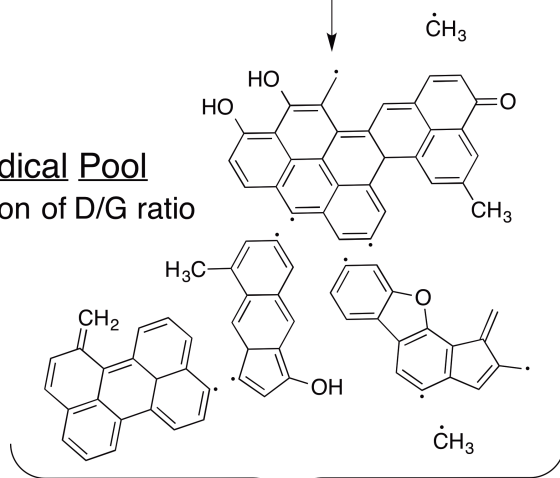
Figure 12: D/Gr ratio with ball-milling time

Biochar Feedstock



Ball-Milling

Radical Pool
Reduction of D/G ratio



Locally Organized Structures

Figure 13: Proposed ball-milling reaction steps

Electron Spin Resonance Spectroscopy (ESR)

A key step in the hypothetical mechanism described in Figure 13 is the initial accumulation of radical bearing defect sites. Since the radical content of samples can be measured independently of their vibrational structure, experiments to quantify the radical content of the ball-milled char provide a means to test the Figure 13 hypothesis. Electron Spin Resonance (ESR) was chosen for this task due to its high sensitivity for detecting unpaired electrons, as well as the availability of a suitable instrument at Clark University.

Figure 14 shows the ESR spectra obtained from three different ball-milled samples. With increasing ball-milling time the radical peak intensities and peak areas increase as well. These increases can be attributed to a rise in amount of radicals within the sample as a result of ball milling. This trend was expected based on comparison with prior work done by Smith et al. where ball-milling of graphite showed increased radical content due to the creation of radical bearing edge sites in the graphitic plane³⁵

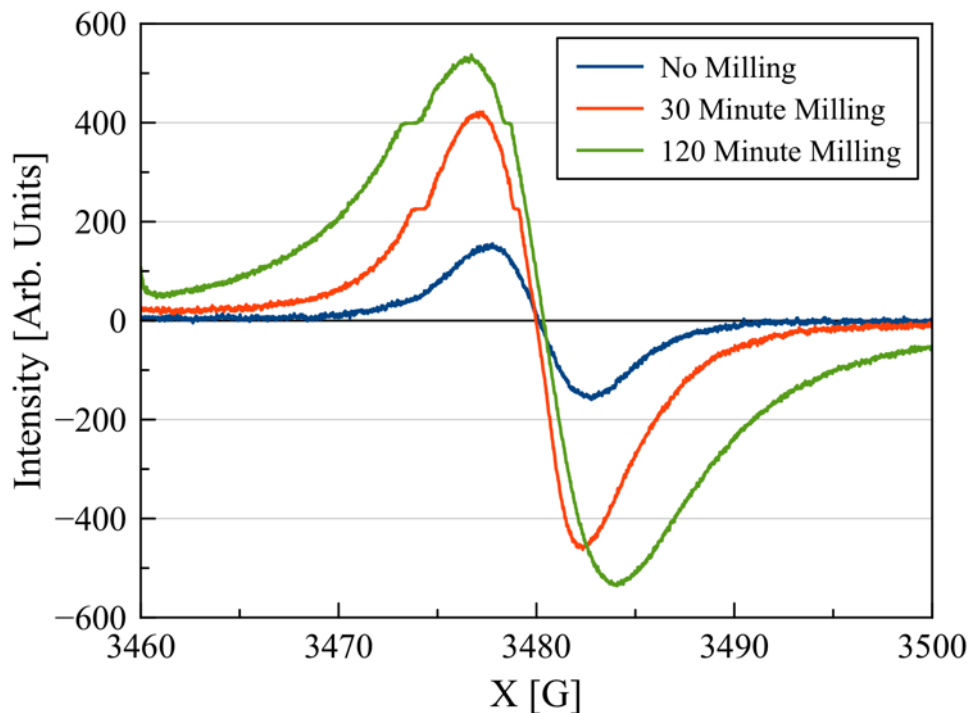


Figure 14: Progressive changes in observed ESR spectra of ball-milled char samples

Figure 14 contains qualitative information on radical composition. Specific free radicals are represented by the minor bumps in the peaks of the 30-minute and 120-minute ball milled samples. On the other hand, they are non-existent in the 0-minute and 30-minute spectra.

Data obtained from the ESR experiments was quantified and plotted in Figure 15 by normalizing the integrated spectrum areas to their respective masses. Figure 15 displays the trend obtained which shows an increase in radical content with ball-milling time. Of note is the difference between the new and old sample of 30 minute ball-milled char. Figure 15 shows that the older biochar sample has lower radical content, indicating that radical sites continue to form stable structures after ball-milling is stopped. Further ESR experiments are needed to verify these results and identify clear trends in radical bond reforming. This result however, made a Raman study of time after ball-milling a valuable next step in understanding the radical presence in ball-milled biochar.

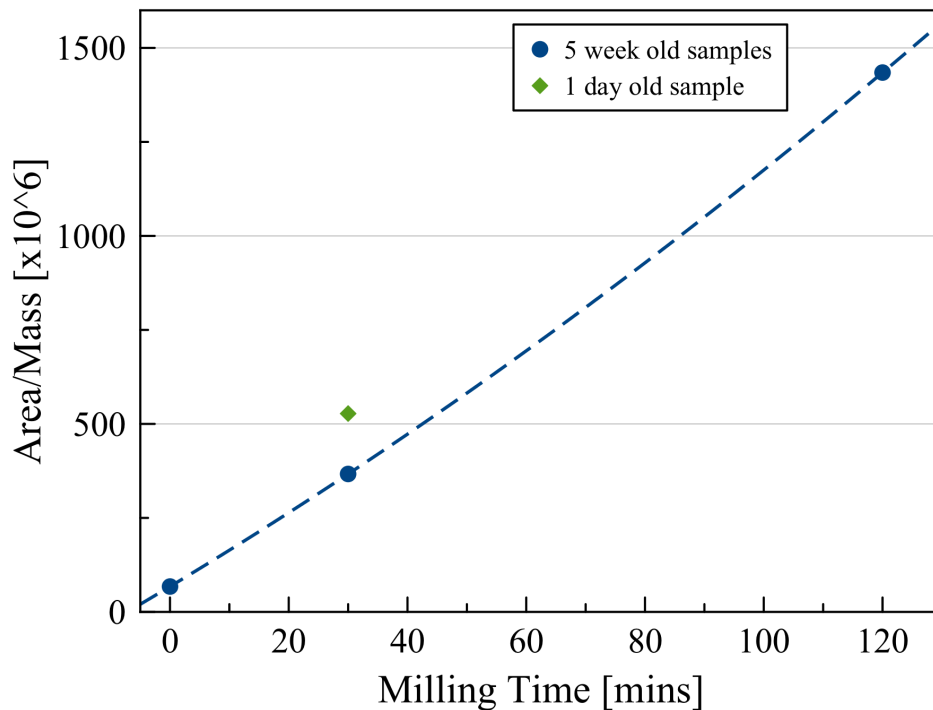


Figure 15: Normalized radical content increases with ball-milling

Defect Stability Study

The defect stability study aimed at understanding the short and long-term effects of ball-milling by monitoring a single location in a biochar sample and observing the changes in its Raman spectrum over time. The same peak ratio analysis as in the ball-milling time study was carried out.

As discussed previously, the $D/(G_R+V_L+V_R)$ can provide information on the relative change from amorphous, short aromatic chains of less than 6 aromatic rings into the more locally organized 6+ aromatic chains. Figure 16 plots the $D/(G_R+V_L+V_R)$ ratio as a function of time elapsed following ball milling. Figure 11 showed a decrease of short ring chains with milling time while Figure 17 shows that after milling, there is a slight increase in the presence of short aromatic chains. The possibility that the newly formed long aromatic chains are being broken down once more is unlikely, as no force is being applied to them. A likely scenario is that remaining radical sites in short chain aromatics are reforming to configurations similar to their original state, regenerating bridging methyl and methylene groups to connect the aromatic chains. To only compare the aromatic ring quantities, the D/G_R ratio was calculated as shown in Figure 18. The G_R peak can be difficult to fit accurately due to its location near the intense G peak, so Figure 17 has large variability. Despite this, it appears that the general trend is one of increasing D peak area, indicating an increase in larger aromatic structures.

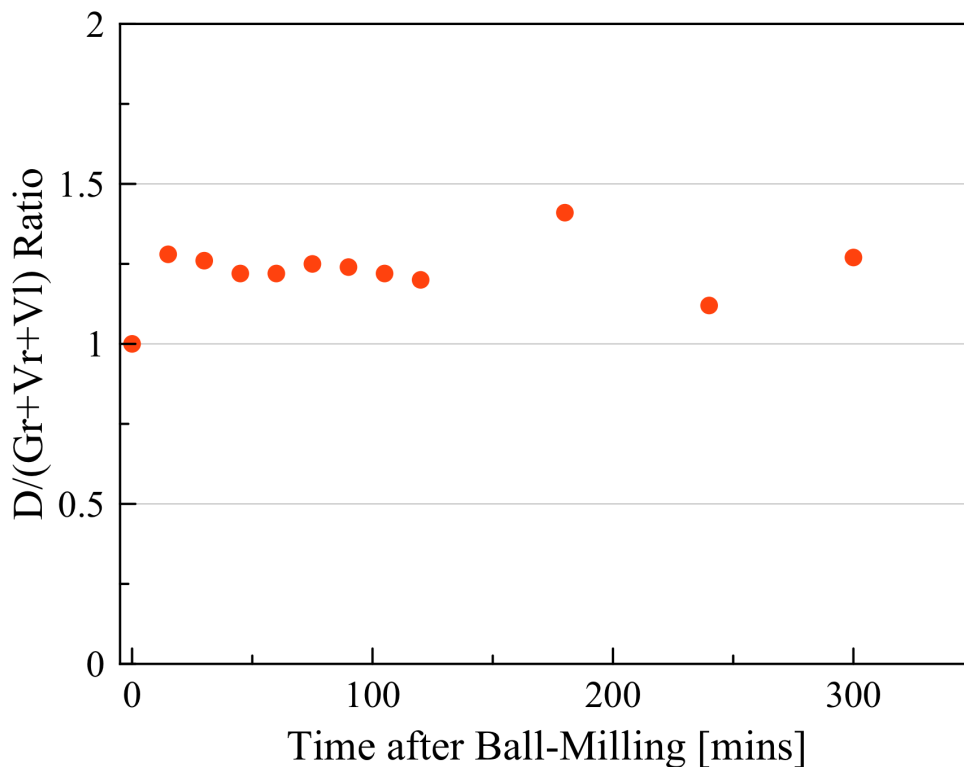


Figure 16: Gr, Vl, and Vr bands compared with D bands

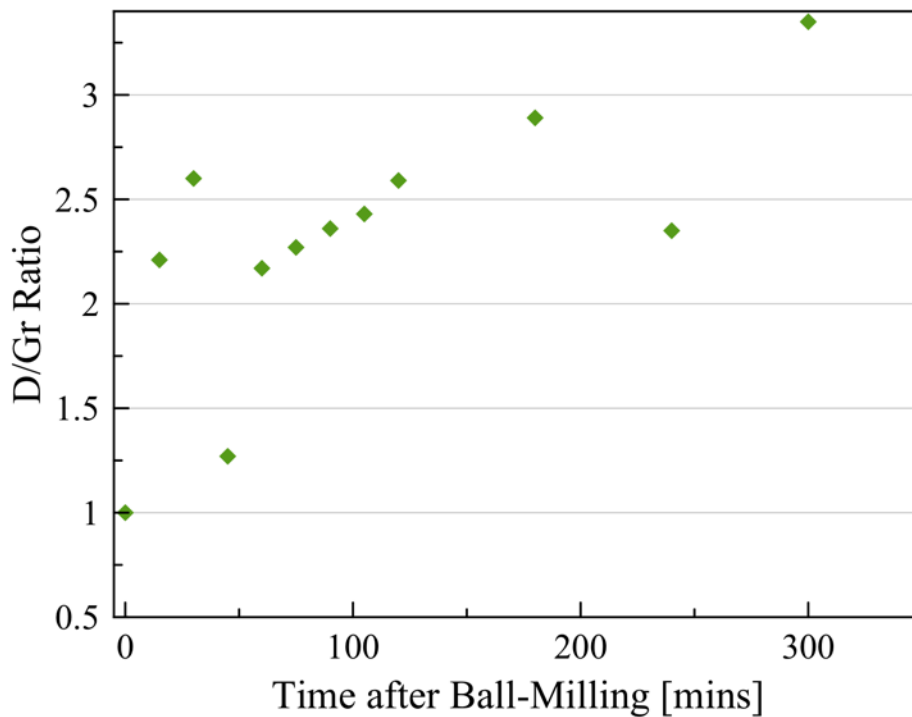


Figure 17: Ratio of the D band vs the G_R band

Upon first inspection, the increase in D peak area may appear to contradict Figure 16 which shows an increase in short aromatic chains. This however, may not be the case when considering the large presence of radicals that was detected in the ESR study. It seems more likely that the changes in ratios observed in the defect stability study are caused by the reformation of the radical pool into more stable structures rather than a change in the already present stable biochar molecules.

Unlike the study on ball-milling time, the defect stability study does not have a large number of data points to base results off from. To verify all the trends observed regarding defect stability, additional experiments should be run to understand the variability of data seen in the two stability experiments that were carried out. The next section of this report will present some recommended next steps in developing a more accurate model of the biochar ball-milling process.

Recommendations

The results obtained from this study have provided valuable insight into the mechanisms that affects biochar during ball-milling. That being said, there are still questions left unanswered as well as new questions that have arisen from the obtained results. It is therefore crucial to analyze the areas of uncertainties within the study and address methods to improve the study of ball-milling for future projects.

Char Synthesis

As seen in the results section of the char synthesis, the visual appearance of the char itself varied from batch to batch variations. There are a few improvements to make the char more uniform. One recommendation would be to get an oven with a timer and an accurate temperature control to make sure the char is synthesized at the same conditions every time. If possible, one batch of char should be used for each study. This would require making more biochar each time, but it should improve the quality of the results by avoiding char feedstock variability within a single experiment. An additional improvement would be to explore how the original char is affected by varying oven time, oven temperature, and the ethanol/water washing procedure used. The current procedure was obtained from (reference), but no procedure optimization was done to determine what factors cause char variability. Understanding these factors would aid in streamlining biochar feedstock synthesis.

Time Study

Despite the number of repeat experiments carried out for the time study, there are still significant variations in the data. To fully understand the real trends that are seen in the time study, a larger sample of experiments should be carried out. As mentioned previously, each new time study should be run with a single batch of biochar to ensure that the observed variations in the feedstock do not skew the Raman spectra. Besides repeating experiments, ball-milling for more than 5 hours can provide new information regarding trends occurring within the char structure. It is possible that the structural changes caused by ball-milling become increasingly significant once a large radical presence is achieved. Figure 11 and 12 in the time study show that before 200 minutes, the changes in peak ratios were small compared to later times. Longer milling times could help clarify this possibility.

It is also important to add more data points to the time study between 90 and 300 minutes, as this can show with more certainty what type of trend is seen in the change in peak ratios. Studying samples between 0 and 30 minutes would also show insight on the crucial radical-creation phase of the milling process. Knowing the minimum time need for a significant radical presence to be observed could be of great use in future studies involving in-situ reactions such as sulfonation.

Improving the peak fitting of the Raman spectra is also of vital importance to obtain clear, accurate data. As seen in Figure 4, the D band area shows overlap between several peak bands which makes peak fitting a difficult task. Obtaining Raman data that minimizes ambient noise and undesired vibrations could be a next step in using Raman as an analytical tool. Cryogenic Raman could reduce the noise obtained from room-temperature molecular vibrations, which in turn may show clearer peak locations in the Raman spectra. Besides this possibility, Raman can be done with many different laser wavelengths and these can provide previously untapped information about the ball-milling process. UV and IR Raman can show different aspects of the same sample and, combined with the current information gathered with visible light, can yield a more complete picture of biochar ball-milling. UV Raman for instance, has been used to reduce the effect of hydrogen content in obtained spectra, improving signal-to-noise ratios and baseline correction requirements.⁴⁰

Studying different parameters of the ball-milling process may also be a tool to develop optimal conditions for processing biochar into an effective catalyst. Altering the milling frequency could show whether the instantaneous energy given by the ball-mill to the sample is more important than the total energy imparted in a ball-milling run. Using a lower frequency than 60Hz may provide too little energy per impact to chemically modify char, even with longer milling times. The ball configuration could also be revisited to determine an optimal ball-milling method. The setup seen in Figure 1 was used based on the work by Immohr, et al¹⁹ but it may be further optimized for ball-milling biochar.

ESR

A crucial first step in improving ESR studies is increasing the studied sample size. The ESR previously described had no repeat experiments, and thus no information on the radical presence variability was obtained. Repeating already-done experiments will provide important information to clarify current results. Methods of improving ESR experiment results would include using freshly ball milled char samples rather than samples that have been milled a month prior. Samples may undergo structural and electronic changes during storage after ball milling and performing ESR on freshly milled samples would reduce this potential source of uncertainty. Another technique is to introduce a radical scavenger, such as TEMPO, in the ball milling process to accept any free radicals that are formed. Figure 18 shows TEMPO's molecular structure.

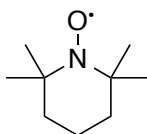


Figure 18: TEMPO Radical Scavenger

If the scavenger prevents the formation of the radical pool, then the peak ratios may greatly differ from the observed results. This would require additional steps to remove the TEMPO from the milling vessel. Milling the char under a nitrogen atmosphere could improve the free radical presence within each sample by restricting oxygen from reacting with those produced radicals. This could be done by milling inside a glovebox or creating a nitrogen flow in the ball-mill. The sample would then be collected and placed in the ESR tubes under the inert atmosphere to ensure as little contact with air is permitted.

A future study that could be performed would focus on free radical degradation within the ball-milled char. This study would consist of ball milling char for a specific amount of time, yet varying the time after milling on which the ESR readings are conducted. This technique could provide insight on the potential deactivation that the free radicals experience from being left idle for some time. Also, x-ray fluorescence would be useful in detecting any metal presence within samples that have been ball milled for extended periods of time to improve the understanding of ESR data. Metal presence within the samples could be disregarded if milling jars made of titanium or ceramic were used rather than stainless steel.

Defect Stability Study

Since only two runs were completed fully for the defect stability study, more runs will need to be completed to fully be able to draw conclusions from the results. In addition to these studies, other types of experiments should be conducted. One would be looking into the effects of the laser on the biochar. To make the stability study as consistent as possible, the Raman spectra were taken at the same spot for every scan. The laser was turned off in between scans, but the laser could have an effect on the char over time, exploring this effect would add to the accuracy of the obtained data. An additional defect stability study inside a nitrogen cell would be useful to compare current results to char unaffected by oxygen exposure.

Future Directions

The observed effect of ball-milling on biochar appears to be based on the creation of a radical "pool" in the early stages of milling. Once a critical amount of defect sites has been created, they are numerous enough to begin reacting within themselves. This accumulation period generates the observed lag time in the time study plots. With this information, a future direction of the project would be to exploit this radical pool before it begins to react with other biochar molecules. As mentioned before, in-situ sulfonation of the char could be a good first experiment to attempt. There are several other sulfonation procedures such as fuming sulfuric acid or an acid bath that may be used as references to compare the effectiveness of ball-milled functionalization. An interesting factor of in-situ sulfonation is the fact that little sulfuric acid may be required instead of the concentrated acid required for other methods. Solid acids such as toluenesulfonic acid could also be used, which would avoid complicated cleaning procedures. Succeeding in ball-milled sulfonation of biochar could be a crucial next step in carbon-based catalyst production.

Once sulfonation has been achieved, catalyst characterization should be carried out. Possible analyses should include the measurement of acid sites, surface area and stability. Boehm titration could be used to measure acid sites, as this method can differentiate between different acid groups. BET surface area measurements can provide additional information to determine the effectiveness of the catalyst, though it is likely that the amorphous structure of the char would make the material have little porosity. Finally, testing the catalyst with a

representative reaction such as alcohol dehydration could show both the potential activity of the catalyst as well as its stability in a reaction medium.

Conclusion

This first look at the potential of ball-milling as a green catalyst preparation tool was primarily an investigation of the chemical changes that occur during ball-milling and how to quantify them. An analytical procedure to monitor the changes caused by ball-milling was developed using Raman spectroscopy that allows for short scanning times. This proved crucial in understanding the time dependency of the chemical changes that take place during biochar ball-milling. Ball-milling produces forces strong enough to create defects in biochar that form a radical pool. After extended milling times beyond 200 minutes, the radicals begin to noticeably react to form new locally organized biochar structures. Electron-spin resonance studies showed how the radical pool significantly increases with ball-milling time. Future studies may provide insight on the stability of the radical pool. Once ball-milling stops, the newly formed structural changes made to the biochar remain relatively stable. Raman studies performed hours after milling suggest remaining radical pool however, continues to form stable structures after processing, albeit at a slower pace than during extended ball-milling. The study showed that ball-milling times on the order of hours may be suitable for catalyst functionalization, as extended ball-milling causes the radical pool to form locally stable molecules. Harnessing the reactivity of the radical pool before this stabilization process commences would allow for a new tool for catalyst preparation. Future studies using ball-milling functionalization may assist in the production of carbon-based catalysts following the principles of green chemistry.

Acknowledgements

We thank Professors Michael Timko and Geoffrey Tompsett for their guidance and assistance throughout this research project. Professor Frederick Greenaway allowed us to perform ESR studies on his instrument at Clark University. Additionally, we thank Andrew Butler and Doug White for their instrumentation support.

Works Cited

1. *Climate Change 2013: The Physical Science Basis*; Intergovernmental Panel on Climate Change: Geneva, Switzerland, 2013.
2. *World Fossil Fuel Reserves and Projected Depletion*; Colorado River Commission of Nevada: Nevada, 2002.
3. Monthly Energy Review: March 2013. Energy Information Administration, Ed. Department of Energy: 2013; p 158.
4. Dunford, N. T., *Lignocellulosic Biomass Processing*. Wiley - Blackwell: Oxford, UK, pp 293-311.
5. Bridgwater, A. V.; Peacocke, G. V. C., Fast pyrolysis processes for biomass. *Renewable and Sustainable Energy Reviews* **2000**, *4* (1), 1-73.
6. Ormsby, R.; Kastner, J. R.; Miller, J., Hemicellulose hydrolysis using solid acid catalysts generated from biochar. *Catalysis Today* **2012**, *190* (1), 89-97.
7. Dias, A. S.; Lima, S.; Carriazo, D.; Rives, V.; Pillinger, M.; Valente, A. A., Exfoliated titanate, niobate and titanoniobate nanosheets as solid acid catalysts for the liquid-phase dehydration of d-xylose into furfural. *Journal of Catalysis* **2006**, *244* (2), 230-237.
8. Zhang, L.; Yu, H.; Wang, P., Solid acids as catalysts for the conversion of d-xylose, xylan and lignocellulosics into furfural in ionic liquid. *Bioresource Technology* **2013**, *136* (0), 515-521.
9. Alexander, G., *Green Chemistry: Theory and Practice*. *Chemical Engineering Progress* **2000**, *96* (9), 54.
10. Zhang, B.; Ren, J.; Liu, X.; Guo, Y.; Guo, Y.; Lu, G.; Wang, Y., Novel sulfonated carbonaceous materials from p-toluenesulfonic acid/glucose as a high-performance solid-acid catalyst. *Catalysis Communications* **2010**, *11* (7), 629-632.
11. Guo, H.; Qi, X.; Li, L.; Smith Jr, R. L., Hydrolysis of cellulose over functionalized glucose-derived carbon catalyst in ionic liquid. *Bioresource Technology* **2012**, *116* (0), 355-359.
12. Sairanen, E.; Vilonen, K.; Karinen, R.; Lehtonen, J., Functionalized Activated Carbon Catalysts in Xylose Dehydration. *Top Catal* **2013**, *56* (9-10), 512-521.
13. Huang, J. Y.; Wu, Y. K.; Ye, H. Q., Deformation structures in ball milled copper. *Acta Materialia* **1996**, *44* (3), 1211-1221.
14. James, S. L.; Adams, C. J.; Bolm, C.; Braga, D.; Collier, P.; Friscic, T.; Grepioni, F.; Harris, K. D. M.; Hyett, G.; Jones, W.; Krebs, A.; Mack, J.; Maini, L.; Orpen, A. G.; Parkin, I. P.; Shearouse, W. C.; Steed, J. W.; Waddell, D. C., Mechanochemistry: opportunities for new and cleaner synthesis. *Chemical Society Reviews* **2012**, *41* (1), 413-447.
15. Milev, A. S.; Tran, N. H.; Kannangara, G. S. K.; Wilson, M. A., Unoccupied electronic structure of ball-milled graphite. *Physical Chemistry Chemical Physics* **2010**, *12* (25), 6685-6691.
16. Pierard, N.; Fonseca, A.; Colomer, J. F.; Bossuot, C.; Benoit, J. M.; Van Tendeloo, G.; Pirard, J. P.; Nagy, J. B., Ball milling effect on the structure of single-wall carbon nanotubes. *Carbon* **2004**, *42* (8-9), 1691-1697.
17. Yan, L.; Lin, M.; Zeng, C.; Chen, Z.; Zhang, S.; Zhao, X.; Wu, A.; Wang, Y.; Dai, L.; Qu, J.; Guo, M.; Liu, Y., Electroactive and biocompatible hydroxyl- functionalized graphene by ball milling. *Journal of Materials Chemistry* **2012**, *22* (17), 8367-8371.
18. Xing, T.; Sunarso, J.; Yang, W.; Yin, Y.; Glushenkov, A. M.; Li, L. H.; Howlett, P. C.; Chen, Y., Ball milling: a green mechanochemical approach for synthesis of nitrogen doped carbon nanoparticles. *Nanoscale* **2013**, *5* (17), 7970-7976.
19. Immohr, S.; Felderhoff, M.; Weidenthaler, C.; Schüth, F., An Orders-of-Magnitude Increase in the Rate of the Solid-Catalyzed CO Oxidation by In Situ Ball Milling. *Angewandte Chemie International Edition* **2013**, n/a-n/a.

20. Xing, W.; Dunlap, R. A.; Dahn, J. R., Studies of Lithium Insertion in Ballmilled Sugar Carbons. *Journal of The Electrochemical Society* **1998**, *145* (1), 62-70.
21. Sevilla, M.; Fuertes, A. B., The production of carbon materials by hydrothermal carbonization of cellulose. *Carbon* **2009**, *47* (9), 2281-2289.
22. Cheng, H. N.; Wartelle, L. H.; Klasson, K. T.; Edwards, J. C., Solid-state NMR and ESR studies of activated carbons produced from pecan shells. *Carbon* **2010**, *48* (9), 2455-2469.
23. Dehkoda, A. M.; West, A. H.; Ellis, N., Biochar based solid acid catalyst for biodiesel production. *Applied Catalysis A: General* **2010**, *382* (2), 197-204.
24. Tuinstra, F.; Koenig, J. L., Raman Spectrum of Graphite. *The Journal of Chemical Physics* **1970**, *53* (3), 1126-1130.
25. Griffiths, P. R., The Handbook of Infrared and Raman Characteristic Frequencies of Organic Molecules. *Vibrational spectroscopy* **1992**, *4* (1), 121-121.
26. Ferrari, A. C.; Robertson, J., Interpretation of Raman spectra of disordered and amorphous carbon. *Physical Review B* **2000**, *61* (20), 14095-14107.
27. Aydıncak, K.; Yumak, T.; Sinağ, A.; Esen, B., Synthesis and Characterization of Carbonaceous Materials from Saccharides (Glucose and Lactose) and Two Waste Biomasses by Hydrothermal Carbonization. *Industrial & Engineering Chemistry Research* **2012**, *51* (26), 9145-9152.
28. Sevilla, M.; Fuertes, A. B., Chemical and Structural Properties of Carbonaceous Products Obtained by Hydrothermal Carbonization of Saccharides. *Chemistry – A European Journal* **2009**, *15* (16), 4195-4203.
29. *Size Reduction and Homogenization with Mixer Mills*; Retsch: Haan, Germany, 2013.
30. Tommasini, M.; Castiglioni, C.; Zerbi, G.; Barbon, A.; Brustolon, M., A joint Raman and EPR spectroscopic study on ball-milled nanographites. *Chemical Physics Letters* **2011**, *516* (4-6), 220-224.
31. Ferraro, J. R.; Nakamoto, K., *Introductory Raman spectroscopy*. Academic Press: Amsterdam, 1994.
32. Reich, S.; Thomsen, C., Raman Spectroscopy of Graphite. *Philosophical Transactions: Mathematical, Physical and Engineering Sciences* **2004**, *362* (1824), 2271-2288.
33. Li, X.; Hayashi, J.-i.; Li, C.-Z., FT-Raman spectroscopic study of the evolution of char structure during the pyrolysis of a Victorian brown coal. *Fuel* **2006**, *85* (12-13), 1700-1707.
34. Bottani, E. J.; Tascón, J. M. D., *Adsorption by Carbons : Novel Carbon Adsorbents*. Elsevier Science: Burlington, 2011.
35. Smith, C. I.; Miyaoka, H.; Ichikawa, T.; Jones, M. O.; Harmer, J.; Ishida, W.; Edwards, P. P.; Kojima, Y.; Fuji, H., Electron Spin Resonance Investigation of Hydrogen Absorption in Ball-Milled Graphite. *The Journal of Physical Chemistry C* **2009**, *113* (14), 5409-5416.
36. Lee, E. S.; Forthofer, R. N., *Strategies for Variance Estimation. Analyzing Complex Survey Data*. SAGE Publications, Inc.: Thousand Oaks, CA, 2006.
37. Meyer, E. F., A Note on Covariance in Propagation of Uncertainty. *Journal of Chemical Education* **1997**, *74* (11), 1339.
38. Asadullah, M.; Zhang, S.; Min, Z.; Yimsiri, P.; Li, C.-Z., Effects of biomass char structure on its gasification reactivity. *Bioresource Technology* **2010**, *101* (20), 7935-7943.
39. Kuzuya, M.; Yamauchi, Y.; Kondo, S.-i., Mechanolysis of Glucose-Based Polysaccharides As Studied by Electron Spin Resonance1. *The Journal of Physical Chemistry B* **1999**, *103* (38), 8051-8059.
40. Casiraghi, C.; Piazza, F.; Ferrari, A. C.; Grambole, D.; Robertson, J., Bonding in hydrogenated diamond-like carbon by Raman spectroscopy. *Diamond and Related Materials* **2005**, *14* (3-7), 1098-1102.